

**Measuring the Growth of Structure with
Multi-Wavelength Surveys of
Galaxy Clusters**

**Neelima Sehgal
Rutgers University**

**December 18th
Berkeley Cosmology Seminar**

Outline

- Background: Cosmology from galaxy cluster surveys
- Compare X-ray and weak-lensing cluster mass estimates to understand mass estimate biases
- Study cluster sample selection in context of upcoming SZ surveys

Background: The growth of structure as an important cosmological probe

Current precision probes of cosmology (the primordial microwave background, type Ia supernova, and galaxy-redshift surveys) measure the expansion of the Universe

General relativity (GR) provides a relation between the expansion rate and the Universe's matter and energy content

We measure that the expansion of the Universe is accelerating, which implies either

- 1.) the Universe is dominated by some field (dark energy) with negative pressure
- 2.) there is a non-zero cosmological constant
- 3.) GR is incorrect on largest scales

Background: The growth of structure as an important cosmological probe (continued)

Expansion rate alone can not distinguish between dark energy/cosmological constant and a failure of GR

GR provides relation between growth rate of structure and expansion rate of Universe

Any inconsistency between cosmology implied by growth rate and that inferred from expansion history alone could signal breakdown of GR

Whether measurement of growth of structure confirms a dark energy component or uncovers a flaw with GR, both scenarios would require a fundamental revision of our foundational theories of physics

Dependence of Cluster Abundance Evolution on Cosmology

$$\frac{dN}{dM dz}(M, z) = \delta\Omega \frac{dV}{dz d\Omega}(z) \frac{dn}{dM}(M, z)$$

Number of clusters for a comoving volume element $dV/(dzd\Omega)$ for a solid angle $d\Omega$ on sky

$$\frac{dn}{dM}(M, z) = -0.315 \frac{\rho_0}{M^2} \frac{d \ln \sigma_M}{d \ln M} \times \exp \left\{ - |0.61 - \ln(\sigma_M D_z)|^{3.8} \right\}$$

Number density of objects between M and $M+dM$ at z , derived from numerical simulations. Jenkins et al. 2001.

$$\sigma_M^2 = \int_0^\infty dk (4\pi k^2) P(k) W^2(kR(M))$$

Variance of linear density field on scale R

ρ_0 = matter density today; $R(M)^3 = 3M/(4\pi\rho_0)$; $W(k,R)$ = top-hat filter;
 $P(k)$ = matter power spectrum today

$$\delta(z) = H(z) \int_0^{(1+z)^{-1}} \frac{da}{(aH(a))^3}$$

$D_z = \delta(z)/\delta(0) =$ linear growth function

$$N_{ij} = \int_{M_i} dM \int_{z_j} dz \frac{dN}{dM dz}$$

Number of clusters in given mass and redshift bin;
Galaxy cluster survey measures this.
 (Cosmology dependence is in volume element, growth function, and variance of density field.)

Measuring Cluster Abundance Evolution

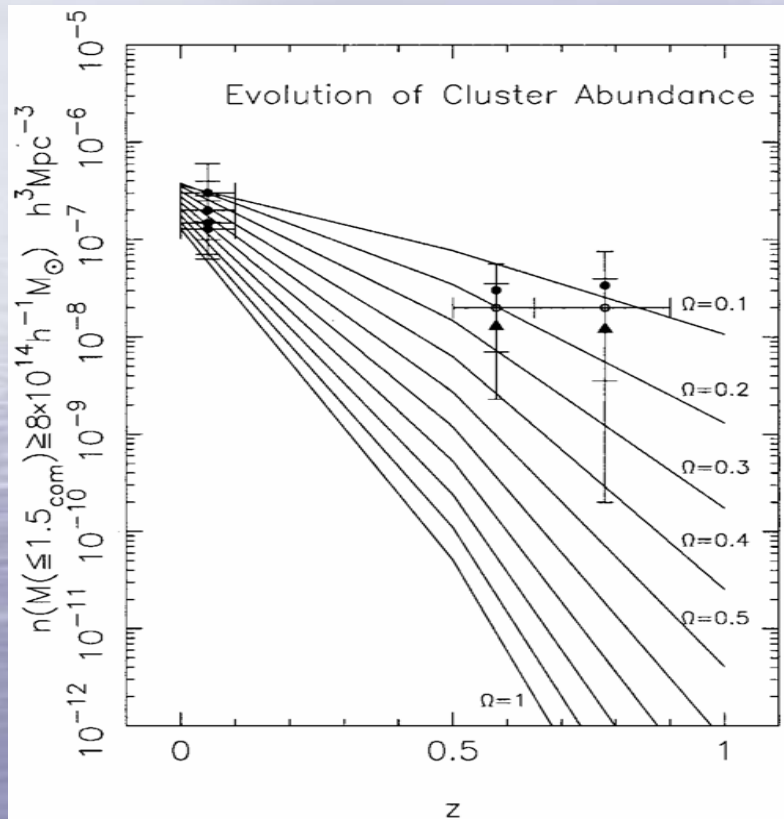
$$N_{ij} = \int_{M_i} dM \int_{z_j} dz \frac{dN}{dM dz}$$

Need to know cluster sample selection and have reliable cluster mass estimates!!

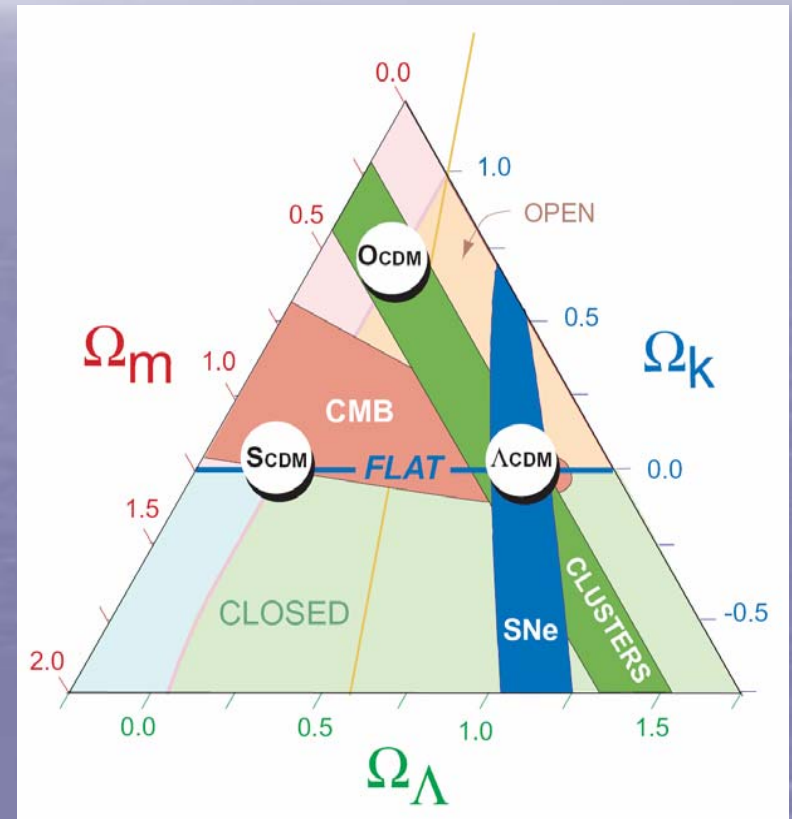
Uncertainties in these will lead to systematic errors in recovered cosmological parameters.

Can study biases and uncertainties in mass estimates and selection function with multi-wavelength cluster surveys and simulations.

Early Cosmological Constraints from Cluster Abundance

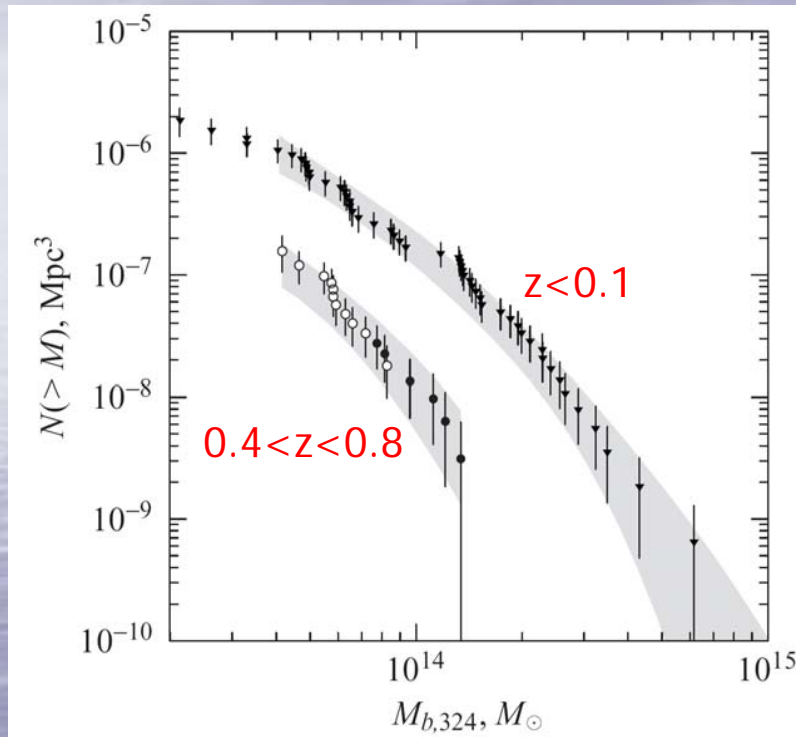


Bahcall and Fan, 1998, PNAS, 95



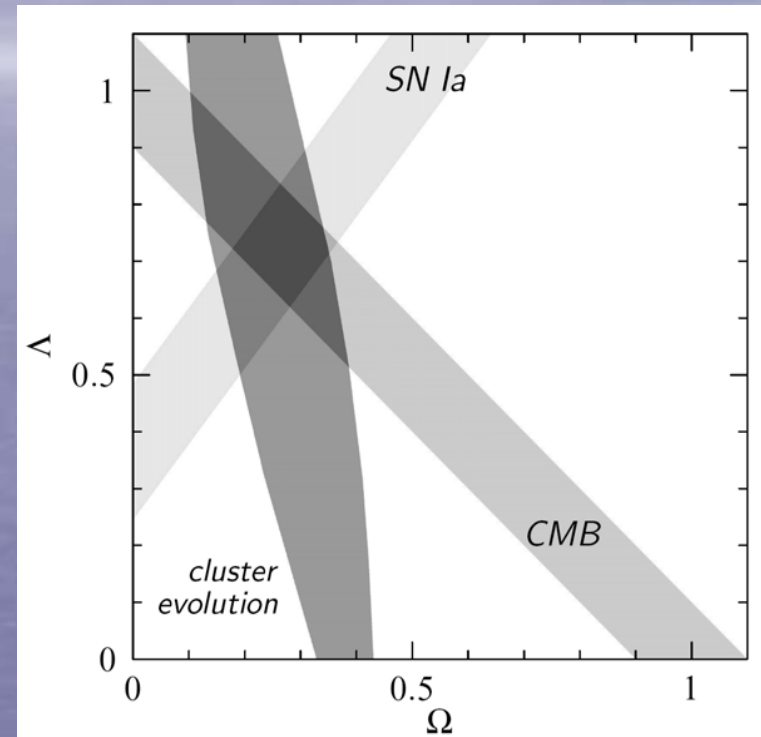
Bahcall, Ostriker, Perlmutter, Steinhardt, 1999, Science, 284

X-ray Constraints



High- z sample: 17 clusters from 160 deg^2 *ROSAT* survey

Low- z sample: 50 brightest X-ray clusters from HIFLUGCS based on *ROSAT* all-sky survey



Cosmological Constraints on Ω_{Λ} and Ω_M

Vikhlinin et al., 2003, *ApJ*, 590

Galaxy Cluster Surveys

X-ray: e.g.

400d *ROSAT* PSPC survey

REFLEX Cluster Survey

Optical: e.g.

MaxBCG from Sloan Digital Sky Survey

Millimeter Wavelength: e.g.

Atacama Cosmology Telescope (ACT)

South Pole Telescope (SPT)

Atacama Pathfinder Experiment (APEX)

Planck satellite

Weak-lensing: e.g.

Deep Lens Survey (DLS)

CFHT (Canada-France-Hawaii Telescope)

Legacy Survey Deep

LSST (Large Synoptic Survey Telescope)

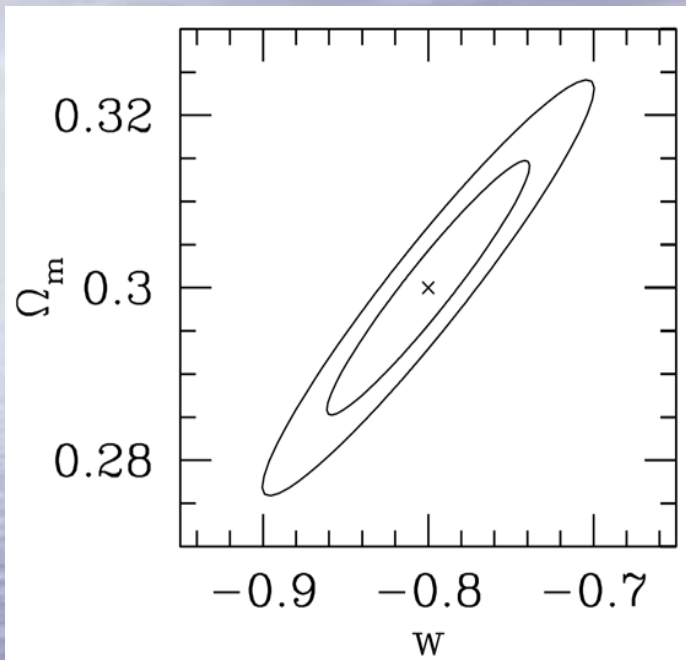
Millimeter (SZ) survey

advantage: SZ signal is independent of redshift

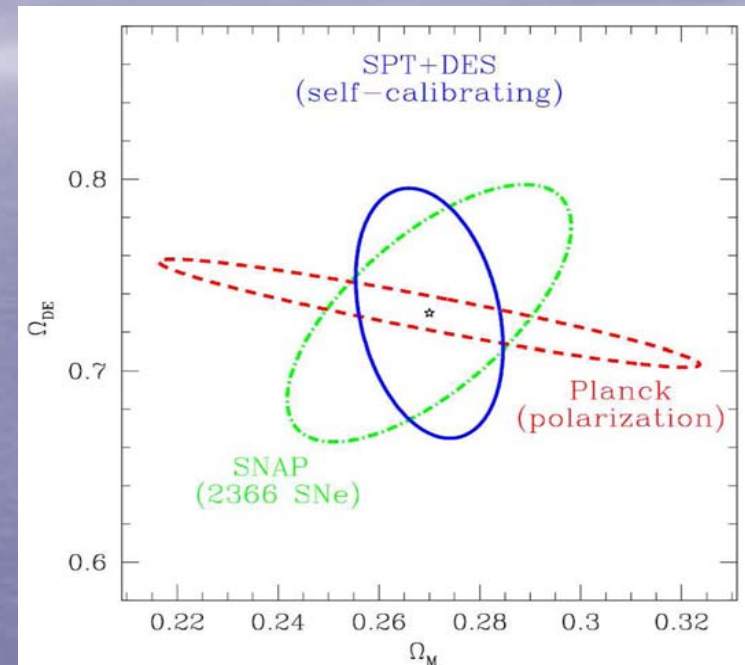
Weak-lensing survey

advantage: gravitational potential directly probed

Expected Cosmological Constraints



Carlstrom, Holder, and Reese, 2002, A&A, 40
Constraints on Ω_M and w given an SZ survey of several thousand sq. degrees assuming all clusters above $2.5 \times h^{-1} 10^{14}$ Msun are found, with redshifts, and **with only statistical errors**.



"SPT White Paper for the Dark Energy Task Force", Carlstrom et al. 2005

Forecast for constraints on Ω_{DE} and Ω_M for SPT+DES using self-calibration. Assumes knowledge of dN/dz , cluster power spectrum, and masses of 100 clusters to 30% accuracy. Includes some, but not all, systematic errors.

Comparison of X-ray and Weak-Lensing Cluster Mass Estimates

This work:

“Probing the Relation Between X-ray-Derived and Weak-Lensing-Derived Masses for Shear-Selected Galaxy Clusters: I. A781”, N. Sehgal, J. P. Hughes, D. Wittman, V. Margoniner, J. A. Tyson, P. Gee, I. Dell’Antonio, *ApJ*, 2008, 672 (to appear)

Compare X-ray and weak-lensing masses for four clusters that comprise the top-ranked shear-selected cluster system in the Deep Lens Survey

System is associated with A781

X-ray observations are from XMM-Newton and Chandra

Weak-lensing observations are from Kitt Peak Mayall 4-m telescope

Goals of this analysis for a larger sample:

To study bias in using cluster baryons as tracers of cluster gravitational potential

To study projection bias that can bias weak-lensing mass estimates

To study bias (or absence of bias) in shear-selection (Up to 20% of shear-selected clusters may not have heated ICM enough to be visible by current X-ray satellites.)

Ratio of $M_{\text{xray}}/M_{\text{weaklens}}$ may be a good diagnostic of the dynamical state of a cluster

Deep Lens Survey (DLS)

DLS: deep BVRz' imaging survey of 20 sq deg; magnitude limit is 25.5 in R band (PI: Tony Tyson; Co-PI's: Dave Wittman, Ian Dell'Antonio)

Observations taken with Cerro Tololo Blanco and Kitt Peak Mayall 4-m telescopes

Goal of survey: study growth of mass clustering over cosmic time using weak lensing

Weak lensing: distortion to shapes of background galaxies by intervening mass

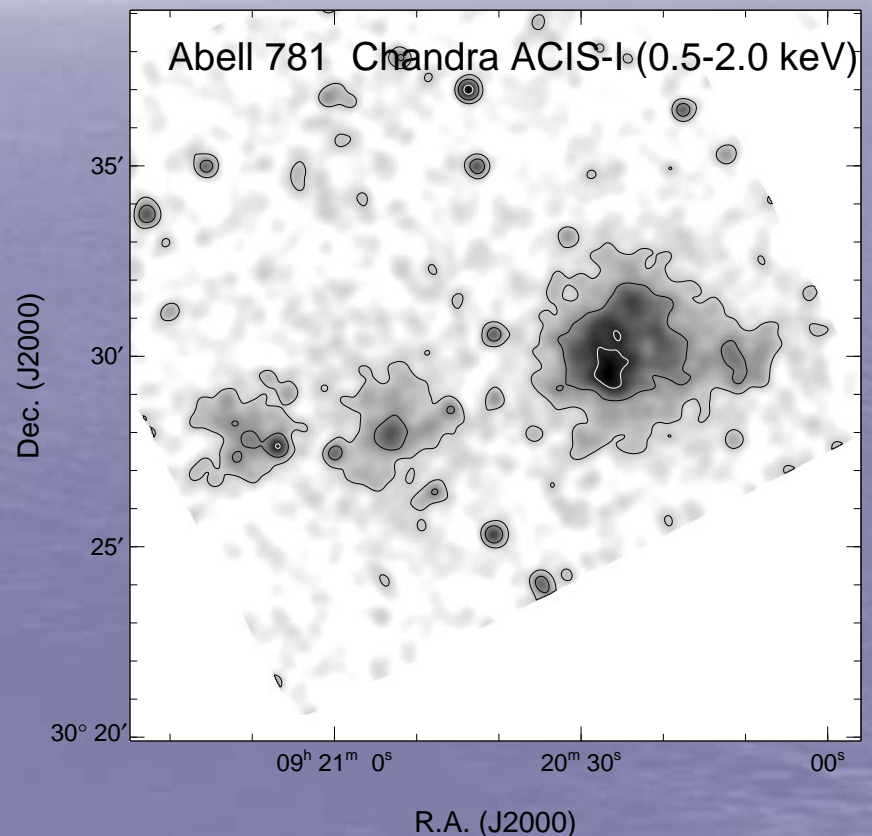
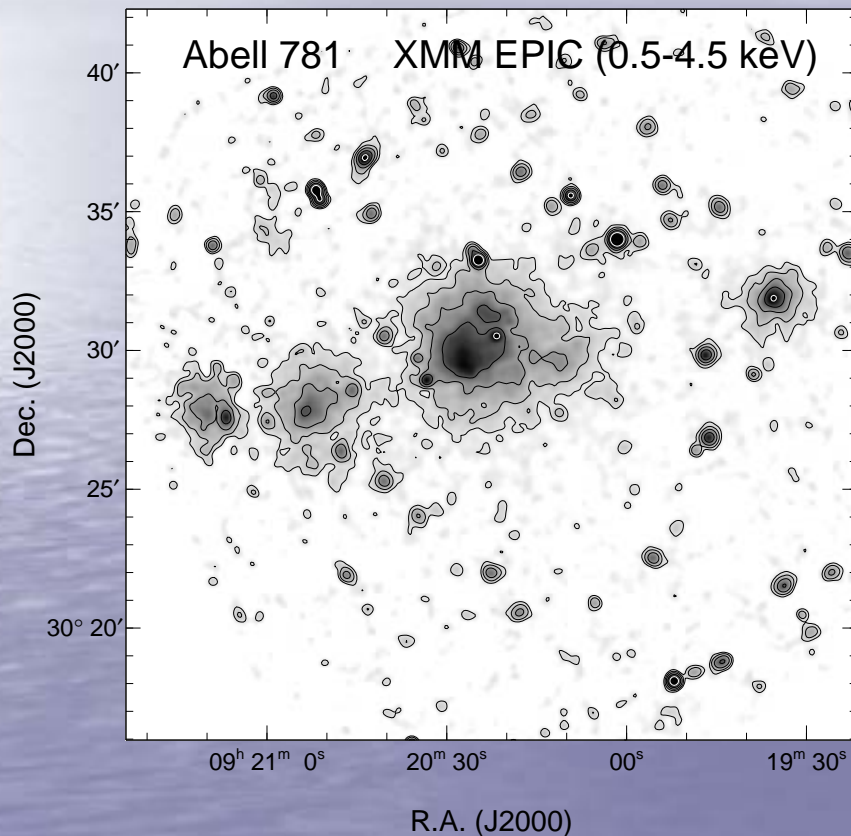
Found > 20 clusters so far, should find ~ 40 when done



FIG. 8.—DLSCL J0920.1+3029 (Abell 781): Convergence map (*green*) and X-ray (*white*) contours overlaid on the multiband optical imaging. North is up, east is to the left, and the field size shown is 17' diameter (4.5 Mpc at $z = 0.298$).

Wittman et al. 2006, ApJ, 643

XMM-Newton and Chandra Images of A781 Cluster Complex



XMM-Newton: 15 ksec; Chandra: 10 ksec

Clusters from left to right are East, Middle, Main, West

Sehgal et al. 2008, ApJ, 672

X-ray Cluster Mass Estimates

Treat gas as a hydrostatic fluid

$$\nabla P = -\rho \nabla \phi(r) \quad \text{where} \quad P = \frac{\rho k T}{\mu m_p}$$

Assume spherical symmetry

$$\frac{1}{\rho} \frac{dP}{dr} = -\frac{d\phi}{dr} = -\frac{GM(r)}{r^2}$$

where $M(r)$ = total mass within r

Rewriting gives

$$M(r) = -\frac{T(r)kr}{G\mu m_p} \left(\frac{d \ln \rho}{d \ln r} + \frac{d \ln T}{d \ln r} \right)$$

X-ray Cluster Mass Estimates

$$M(r) = -\frac{krT(r)}{G\mu m_p} \left(\frac{d \ln \rho(r)}{d \ln r} + \frac{d \ln T(r)}{d \ln r} \right)$$

← Assumes hydrostatic equilibrium

Model cluster gas with a β -model →

$$\Sigma(b) = \int_{-\infty}^{\infty} \epsilon(r) dl \propto \left(1 + \left(\frac{b}{r_c} \right)^2 \right)^{-3\beta + \frac{1}{2}}$$

$$\rho(r) = \rho_{0g} \left[1 + \left(\frac{r}{r_c} \right)^2 \right]^{-\frac{3\beta}{2}}$$

← Surface brightness as a function of projected radius

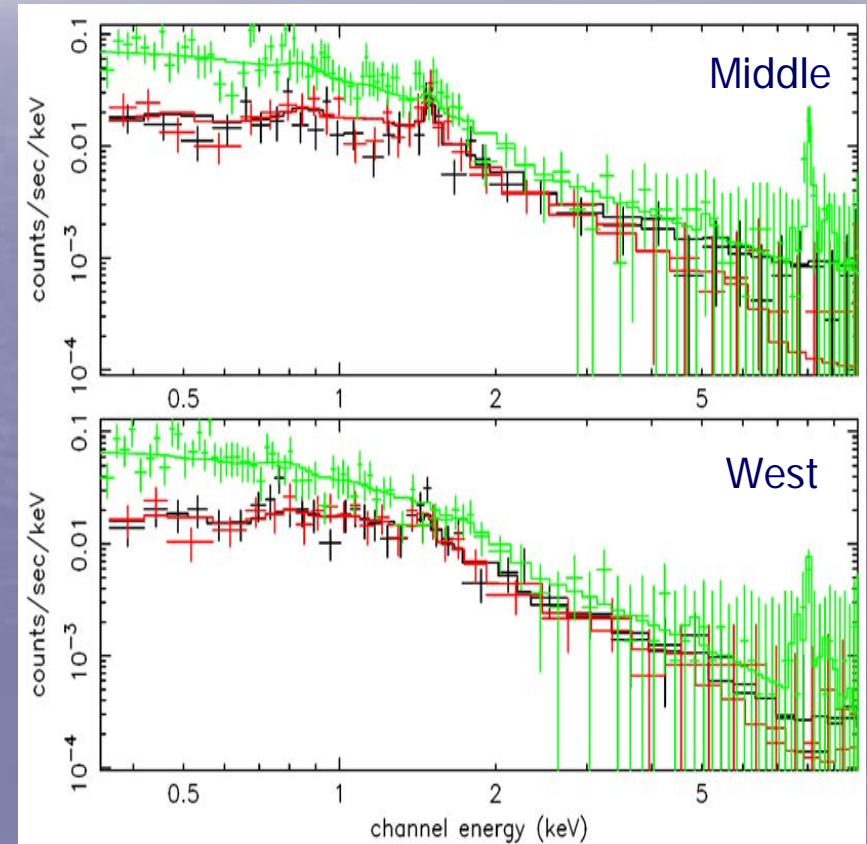
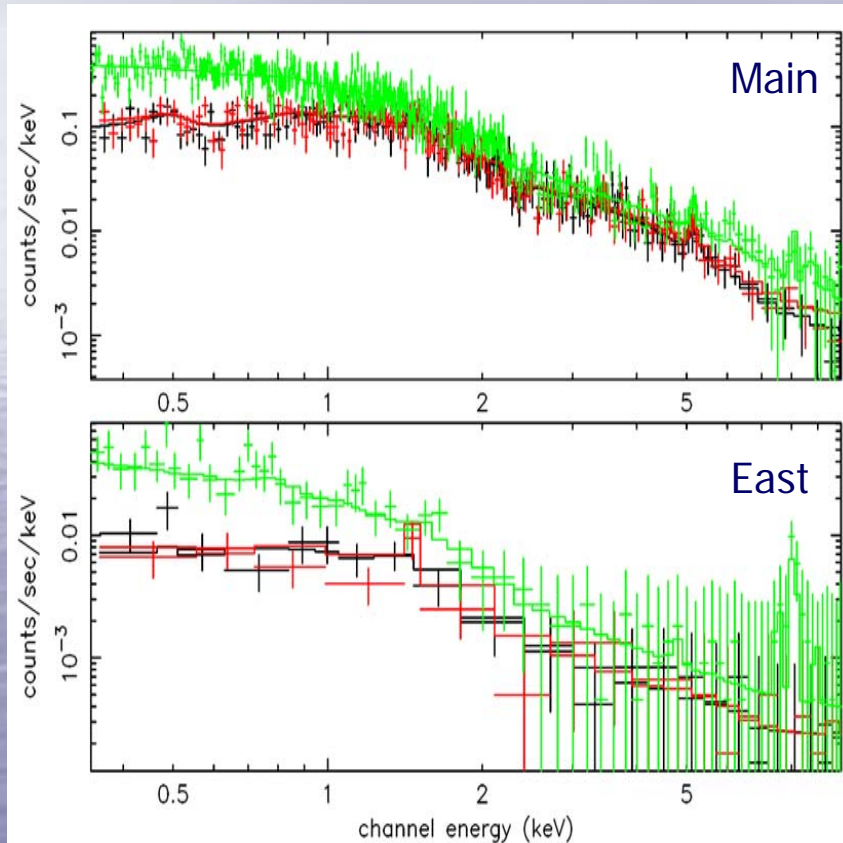
Model dark matter with an NFW profile →

$$\rho_M(r) = \frac{\rho_0}{(r/r_s)(1 + r/r_s)^2}$$

$$M(r) = 4\pi\rho_0 r_s^3 \left(\ln\left(1 + \frac{r}{r_s}\right) + \frac{1}{1 + r/r_s} - 1 \right)$$

← NFW profile gives mass within radius r

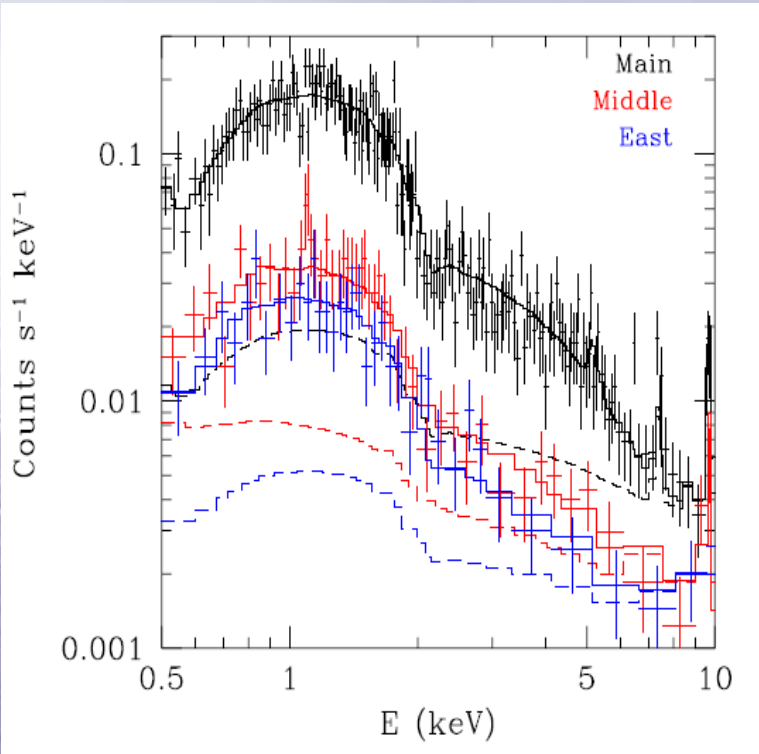
Best-fit to XMM-Newton Spectra



Black = MOS1, red = MOS2,
green = PN instrument on XMM

Sehgal et al. 2008, ApJ, 672

Best-fit to Chandra Spectra



Sehgal et al. 2008, ApJ, 672

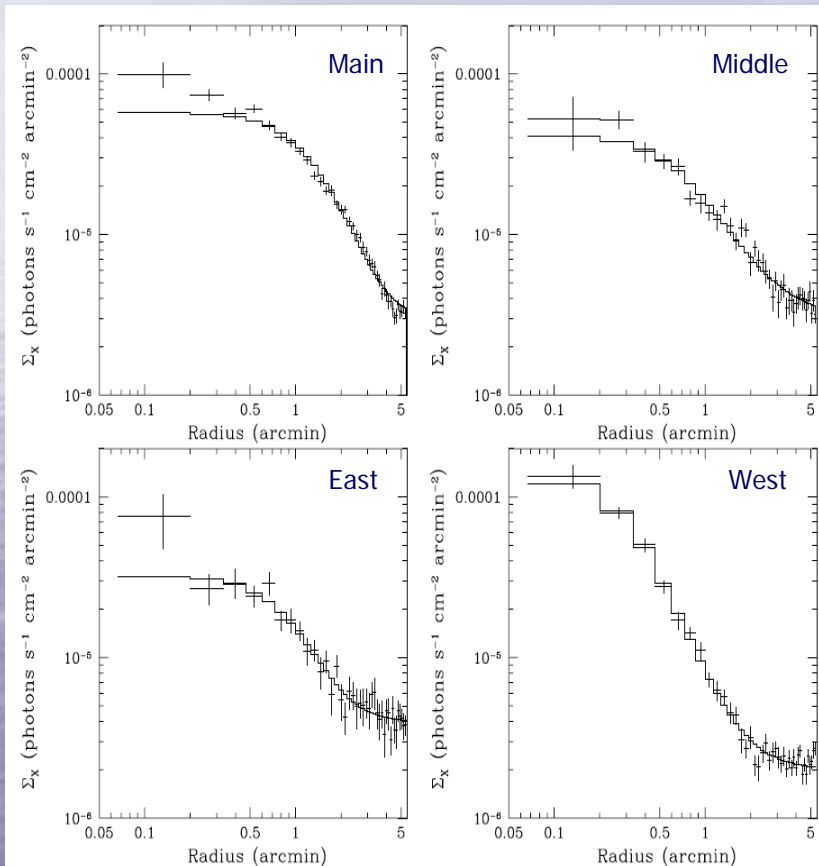
	<i>XMM</i> counts	<i>XMM</i> kT (keV)	<i>Chandra</i> counts	<i>Chandra</i> kT (keV)
East Cluster	505	$3.6^{+0.6+0.6}_{-0.5-0.7}$	300	$4.7^{+1.4}_{-1.0}$
Middle Cluster	1135	$3.7^{+0.4+0.6}_{-0.3-0.4}$	380	$5.0^{+1.6}_{-1.1}$
Main Cluster	8812	$6.3^{+0.3+0.4}_{-0.3-0.3}$	2400	$7.3^{+1.1}_{-0.7}$
West Cluster	1163	$4.0^{+0.4+0.5}_{-0.3-0.5}$	0	...

Best-fit emission-weighted, projected, average temperatures within given apertures from spectral fitting with XSPEC

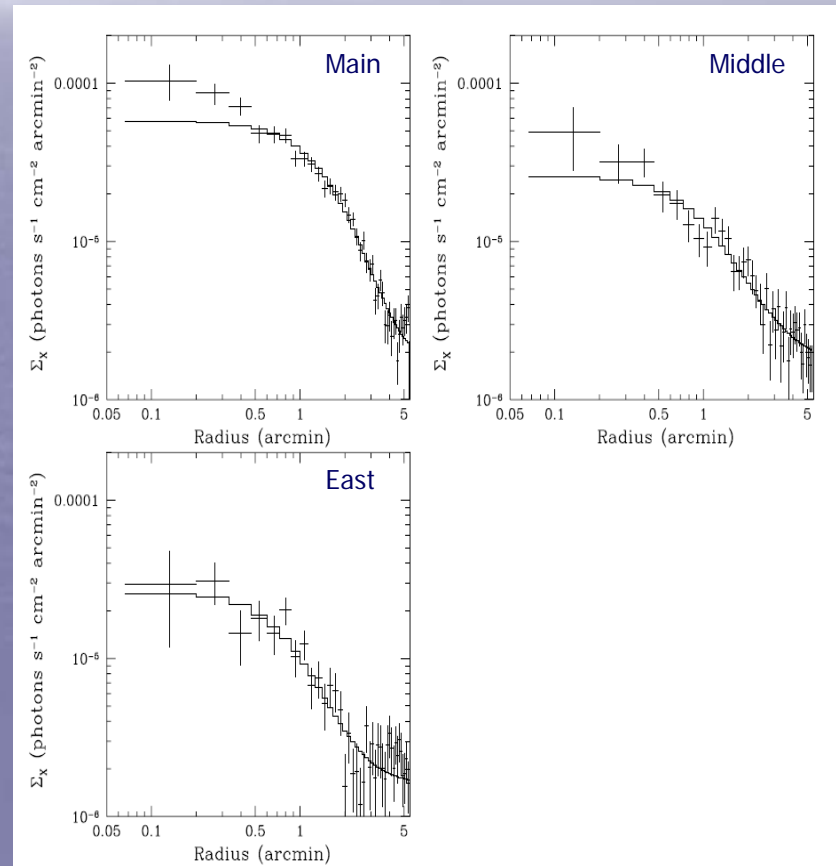
Careful background subtraction was done including using closed observations to model the non-X-ray background in XMM spectra

Fits to Surface Brightness Profiles

XMM-Newton



Chandra



Best-fit β and r_c Values from Surface Brightness Profiles

$$\epsilon(r) \propto \Lambda(T(r))(n_e(r))^2$$

Determined the background surface brightness from the outermost radial bins

$$\Sigma(b) = \int_{-\infty}^{\infty} \epsilon(r) dl \propto \left(1 + \left(\frac{b}{r_c}\right)^2\right)^{-3\beta + \frac{1}{2}}$$

Fixed the background and let r_c , β , and the normalization vary

Best-fit β and r_c values

	<i>XMM</i> β	<i>XMM</i> r_c (arcmin)	<i>Chandra</i> β	<i>Chandra</i> r_c (arcmin)
East Cluster	$0.81^{+0.29}_{-0.15}$	$1.19^{+0.44}_{-0.24}$	$0.68^{+0.39}_{-0.13}$	$0.94^{+0.59}_{-0.29}$
Middle Cluster	$0.51^{+0.05}_{-0.04}$	$0.71^{+0.20}_{-0.15}$	$0.56^{+0.13}_{-0.09}$	$0.99^{+0.49}_{-0.34}$
Main Cluster	$0.87^{+0.06}_{-0.05}$	$1.82^{+0.15}_{-0.15}$	$0.88^{+0.12}_{-0.10}$	$2.01^{+0.34}_{-0.24}$
West Cluster	$0.60^{+0.03}_{-0.02}$	$0.31^{+0.03}_{-0.03}$

Estimated Scale Radius

$$M(r) = -\frac{krT(r)}{G\mu m_p} \left(\frac{d \ln \rho(r)}{d \ln r} + \frac{d \ln T(r)}{d \ln r} \right)$$

$$M(r) = 4\pi\rho_0 r_s^3 \left(\ln\left(1 + \frac{r}{r_s}\right) + \frac{1}{1 + r/r_s} - 1 \right)$$

We need to fix scale radius because data is not deep enough to constrain ρ_0 and r_s .

$$M(r) = 3\beta \frac{kTr}{G\mu m_p} \left[\frac{(r/r_c)^2}{1 + (r/r_c)^2} \right]$$

Estimated mass using an isothermal β -model

$$c(M, z) = \frac{c_0}{1+z} \left(\frac{M}{10^{14} h^{-1} M_\odot} \right)^\alpha$$

Estimated concentration using fitting function from numerical simulations (Dolag et al. 2004, A&A, 416)

$$c = r_{200}/r_s$$

Determined reasonable scale radius.

Exact value of scale radius is not so important for comparison of X-ray and weak-lensing mass estimates.

Key is that we use same scale radius for X-ray and weak-lensing methods, and fit for ρ_0 .

Weak-lensing Shear Map, Best-fit Model, and Residual Map

Exposure: 18 ksec in R band
12 ksec in BVz'

R data has seeing $<0.9''$ FWHM and are used to measure galaxy shapes

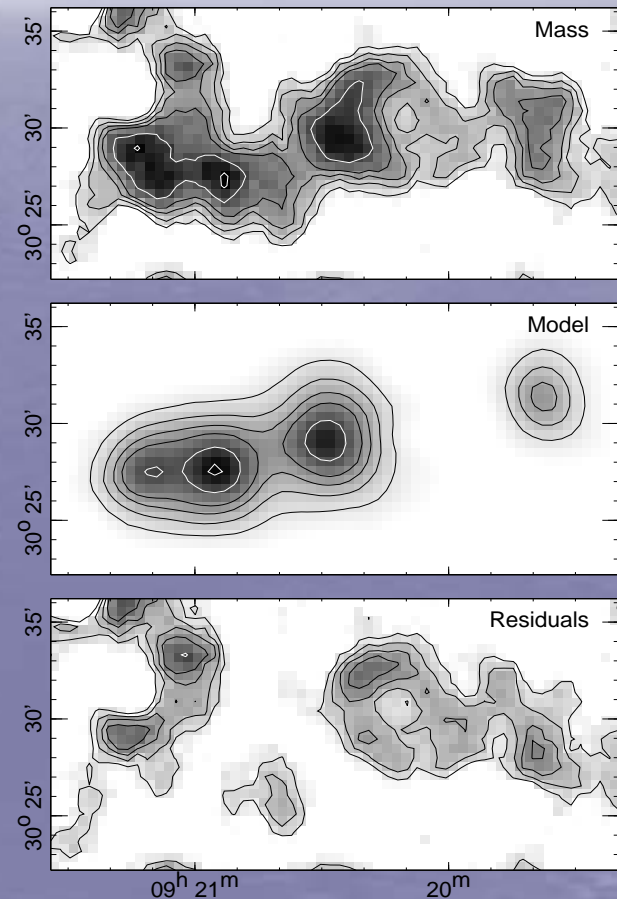
BVz' data used for photometric redshifts

Simultaneously fit axisymmetric NFW profiles to the four X-ray cluster positions

Cluster redshift fixed by spectroscopy

Scale radius (r_s) fixed to value used for X-ray fitting

Fit simultaneously for four ρ_0 values



Results: X-ray vs. Weak-lensing Mass Estimates

	Estimated r_s (Mpc)	XMM ρ_0 (10^{-26} g/cm 3)	Chandra ρ_0 (10^{-26} g/cm 3)	Combined X-ray ρ_0 (10^{-26} g/cm 3)	DLS ρ_0 (10^{-26} g/cm 3)
East	0.37	$3.9^{+1.0}_{-1.0}$	$5.2^{+1.6}_{-1.2}$	4.4 ± 0.8	$4.4 \pm 1.3 \pm 0.6$
Middle	0.31	$5.2^{+1.1}_{-0.7}$	$7.3^{+2.3}_{-1.7}$	5.8 ± 0.9	$6.8 \pm 1.5 \pm 0.8$
Main	0.60	$3.1^{+0.3}_{-0.2}$	$3.5^{+0.5}_{-0.4}$	3.2 ± 0.2	$2.2 \pm 0.4 \pm 0.3$
West	0.33	$6.4^{+1.0}_{-0.9}$...	6.4 ± 1.0	$4.0 \pm 1.7 \pm 0.4$

XMM-Newton and Chandra values are in agreement within 1σ .

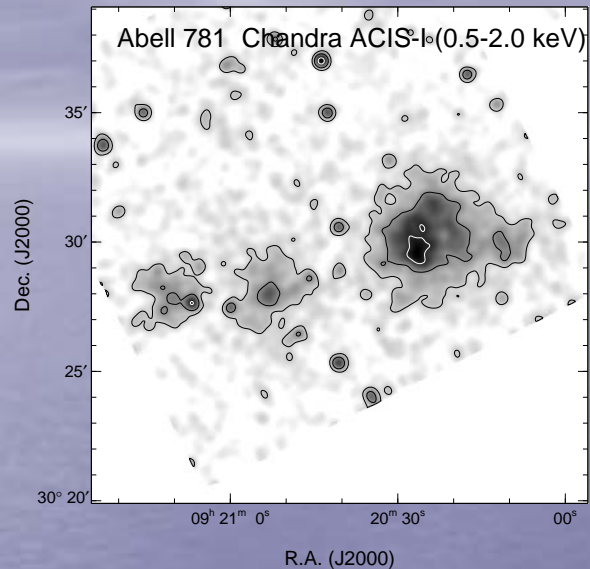
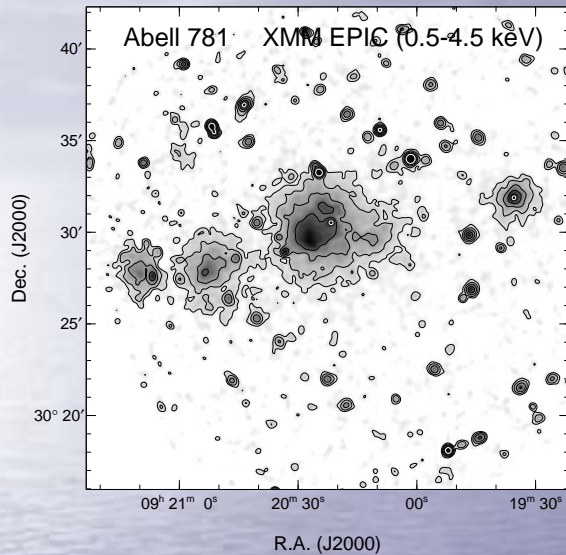
X-ray and weak-lensing central densities, and thus masses, are in agreement for three of four clusters within 1σ .

For the Main cluster, X-ray central density is higher than that from weak-lensing by about 2σ .

	X-ray r_{500} (Mpc)	X-ray M_{500} ($10^{14} M_\odot$)	Weak-lensing r_{500} (Mpc)	Weak-lensing M_{500} ($10^{14} M_\odot$)
East Cluster	$0.74^{+0.06}_{-0.07}$	$1.8^{+0.5}_{-0.5}$	$0.73^{+0.11}_{-0.13}$	$1.8^{+0.9}_{-0.8}$
Middle Cluster	$0.76^{+0.06}_{-0.06}$	$1.7^{+0.4}_{-0.4}$	$0.82^{+0.10}_{-0.12}$	$2.0^{+1.0}_{-0.7}$
Main Cluster	$1.09^{+0.04}_{-0.04}$	$5.2^{+0.3}_{-0.7}$	$0.89^{+0.10}_{-0.12}$	$2.7^{+1.0}_{-0.9}$
West Cluster	$0.79^{+0.06}_{-0.06}$	$2.2^{+0.5}_{-0.4}$	$0.60^{+0.15}_{-0.14}$	$1.1^{+0.8}_{-0.7}$

Sehgal et al. 2008, ApJ, 672

Implications



Main cluster may be merging with subcluster and out of hydrostatic equilibrium.

X-ray mass higher than that from weak-lensing.

Literature:

Cypriano et al. 2004 – 22 X-ray bright clusters; $T_x > 8\text{keV}$ clusters have higher X-ray temps than those inferred from weak-lensing; highest discrepancy for hottest X-ray clusters that showed signs of dynamical disruption.

Kravtsov et al. 2006, Nagai et al. 2007 – hydro sims suggest X-ray temps should be lower for unrelaxed clusters than for relaxed clusters of same mass

Poole et al. 2006, Puchwein & Bartlemann 2007 – X-ray mass estimates can be biased high or low depending on state of merger

Zhang et al. 2007, Bardeau et al. 2007 – 10 X-ray bright clusters; 6 clusters with X-ray/weak-lensing mass discrepancy; half have higher X-ray masses.

Future: We have larger sample of DLS clusters with X-ray data, and we have deeper X-ray data on A781 system.

Cluster Sample Selection for Millimeter-Wavelength Surveys

This work:

“Microwave Sky Simulations and Projections for Galaxy Cluster Detection with the Atacama Cosmology Telescope”,
N. Sehgal, H. Trac, K. Huffenberger,
P. Bode, ApJ, 2007, 664

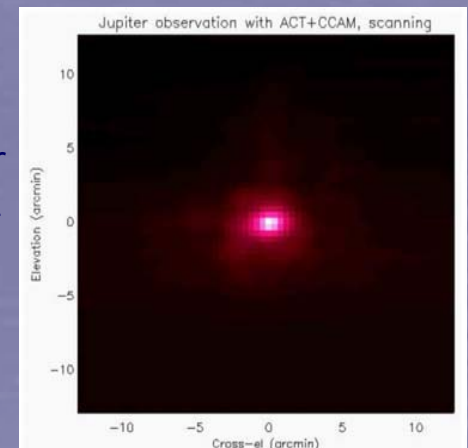
Created large-area sims of the microwave sky to investigate of optimal data reduction techniques; sims are publicly available

Investigated how well three-frequency, arcminute-resolution microwave measurements could detect galaxy clusters via SZ effect; relevant for ACT and SPT



ACT first light image of Jupiter in June 2007-->

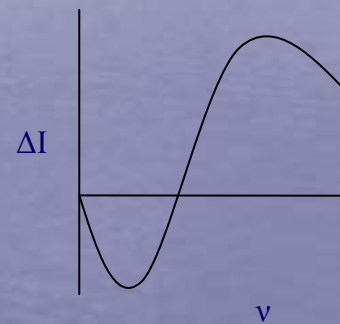
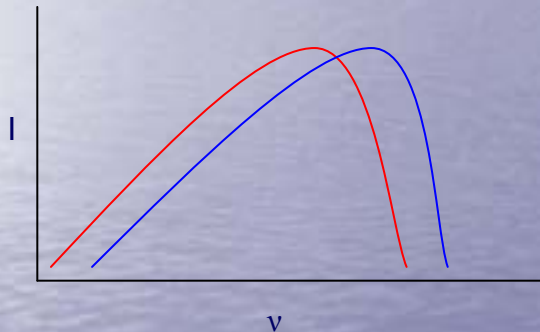
Pictures from ACT website



Thermal Sunyaev-Zel'dovich (SZ) Effect

Inverse Compton scattering of CMB photons off hot electrons in cluster gas

Photons gain an average energy of $k_B T_e / (m_e c^2)$ per scatter

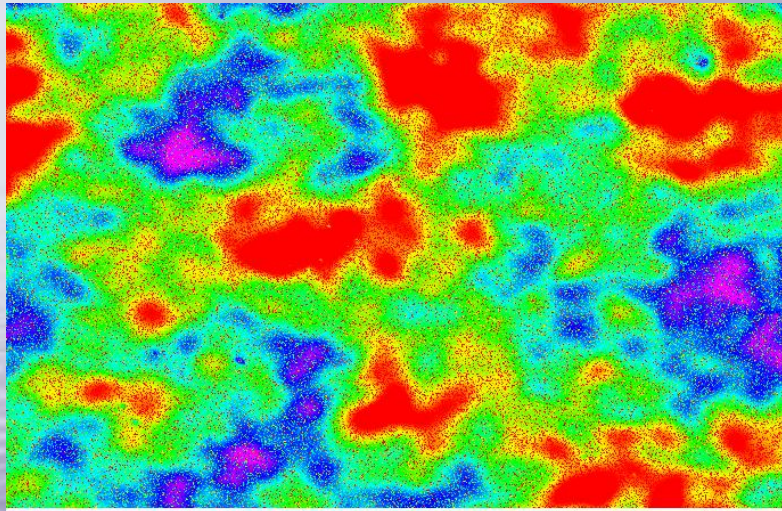


$$\Delta T / T_{\text{cmb}} = g(\nu) \int dl k_B T_e / (m_e c^2) n_e \sigma_T \quad (\text{non-relativistic})$$

This is independent of redshift.

Full SZ effect includes kinetic SZ contribution and relativistic corrections.

Millimeter-Wavelength Simulations



-250 μK

250 μK

Microwave Sky at 145 GHz

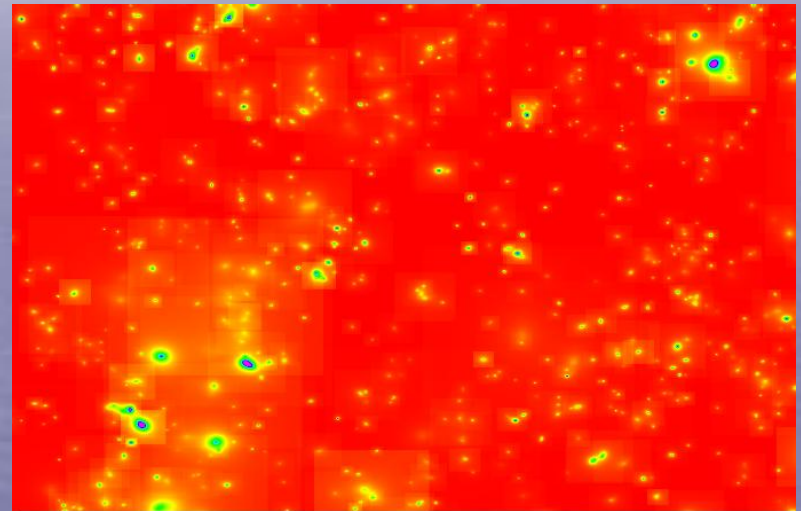
Included components:

primary CMB

thermal & kinetic SZ from ICM

radio & infrared point sources

galactic dust



- 150 μK

0 μK

Thermal SZ signal at 145 GHz

Sehgal et al. 2007, ApJ, 664

Modeling Galaxy Clusters

N-body TPM code

1 Gpc³ box, 1024³ particles

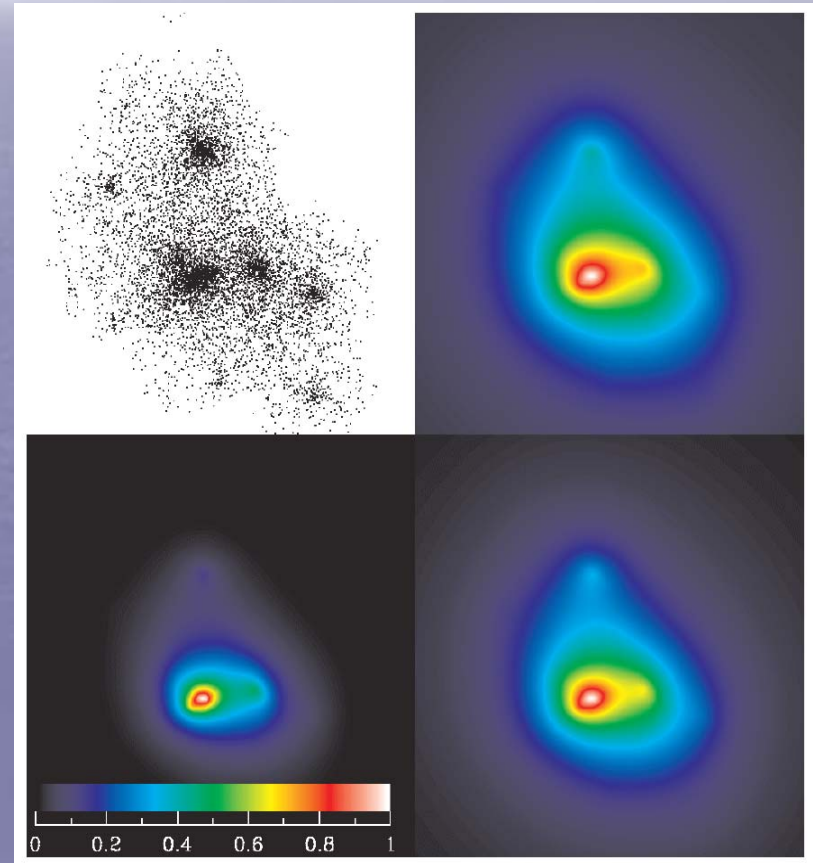
Gas prescription

includes star formation,
feedback, asymmetry

Ostriker, Bode, Babul, 2005

Can vary cluster physics
without redoing expensive runs

- is semi-analytical
- but has physically motivated prescription
- requires calibration with hydro sims and observations



Ostriker, Bode, Babul, 2005, ApJ, 634

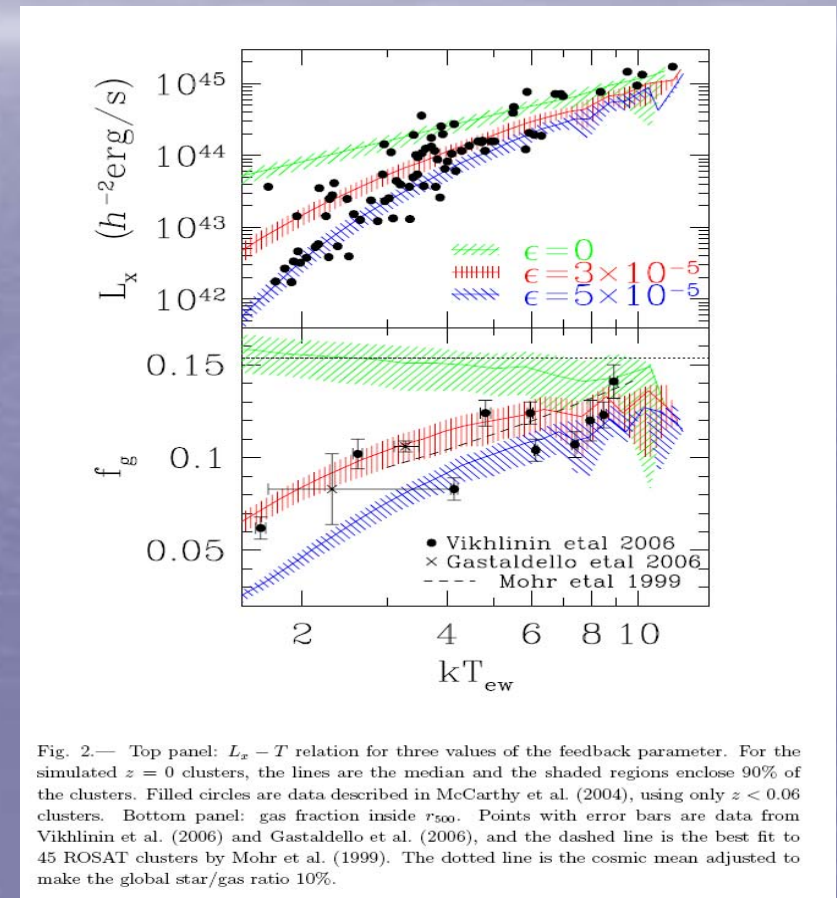
Calibrating Gas Prescription

Feedback from AGN and SN modeled as $\epsilon \times$ rest mass of stars

Feedback efficiency is calibrated off of X-ray observations of nearby clusters

Can generate X-ray and SZ cluster maps and catalogs from N-body sims with small scale cluster physics realistically incorporated

See Bode, Ostriker, Weller, Shaw
ApJ, 663, 2007 for more details



Microwave Sky Simulations

Large area – 2 strips, centered at
-55 and -5 degrees declination,
360 deg around and 4 deg wide

Components include:
clusters $> 5 \times 10^{13} M_{\odot}$

ICM thermal and kinetic SZ with
relativistic contributions

primary CMB

IR and Radio sources –
uncorrelated with clusters

Galactic dust

Halo catalog

Publicly available at

<http://www.astro.princeton.edu/~act/>

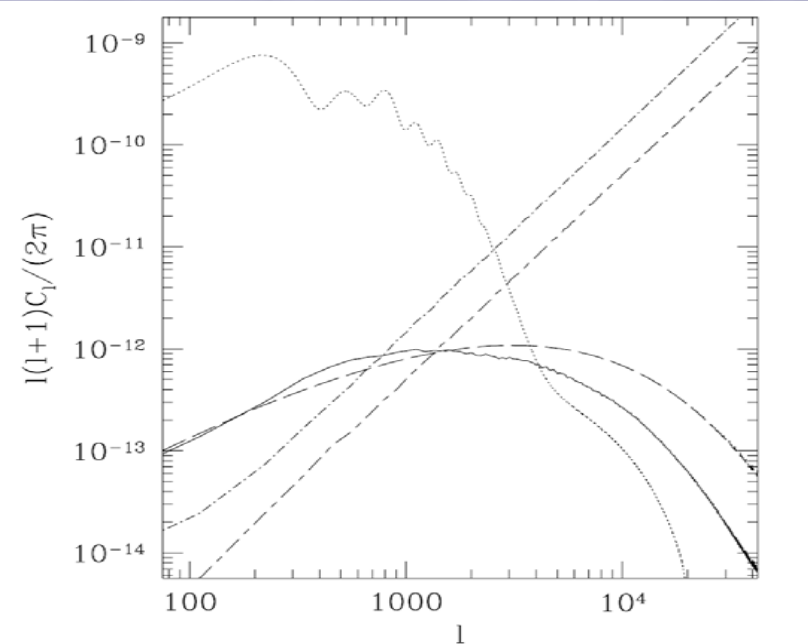


FIG. 3.— Solid curve is the first-order thermal SZ power spectrum at 145 GHz from the simulation. Dashed curve is the first-order thermal SZ power spectrum at 145 GHz derived analytically from Komatsu & Seljak (2002). For comparison, we include the lensed primary microwave background power spectrum derived from CAMB (Challinor & Lewis 2005) for our input cosmology (dotted) and the power spectrum of infrared (dot-dashed) and radio (dash-dashed) point sources from the simulation, also at 145 GHz. The radio source power spectrum includes only sources fainter than 35 mJy. Note that C_l is in dimensionless units of $(\Delta T/T)^2$.

Cluster detection with ACT

- 1'-2' beam, 2-5 uK/beam, 145, 215, 280 GHz channels
- used multi-frequency Wiener filter

Completeness and purity of recovered sample for case with no point sources

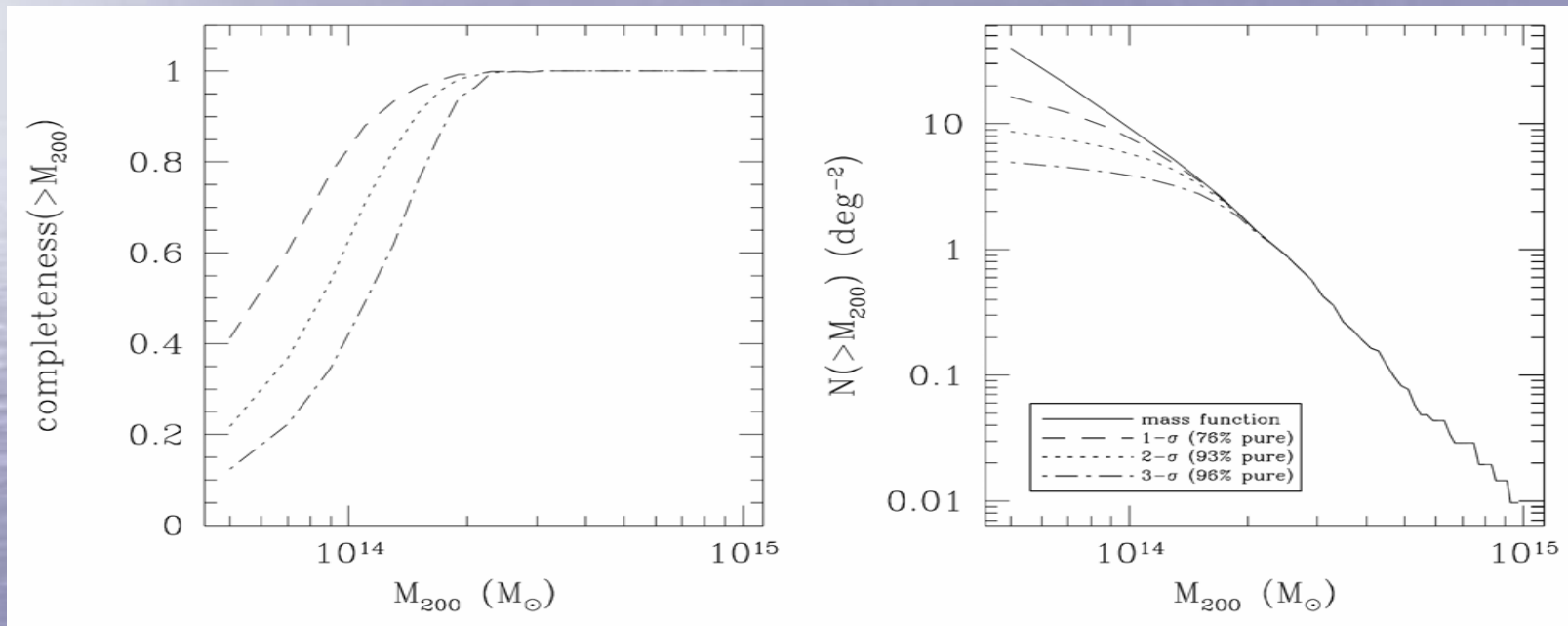


FIG. 7.— Completeness and purity of the detected cluster sample with ACT instrument specifications, in the case of no point sources. Different curves represent 1- σ , 2- σ , and 3- σ threshold cuts in the detection algorithm, where σ is the standard deviation of the filtered map. The solid curve represents the simulation mass function. The purity of each cluster sample is given in the legend. See text for further details.

SZ Cluster Detection

Completeness and purity for case with both infrared and radio point sources

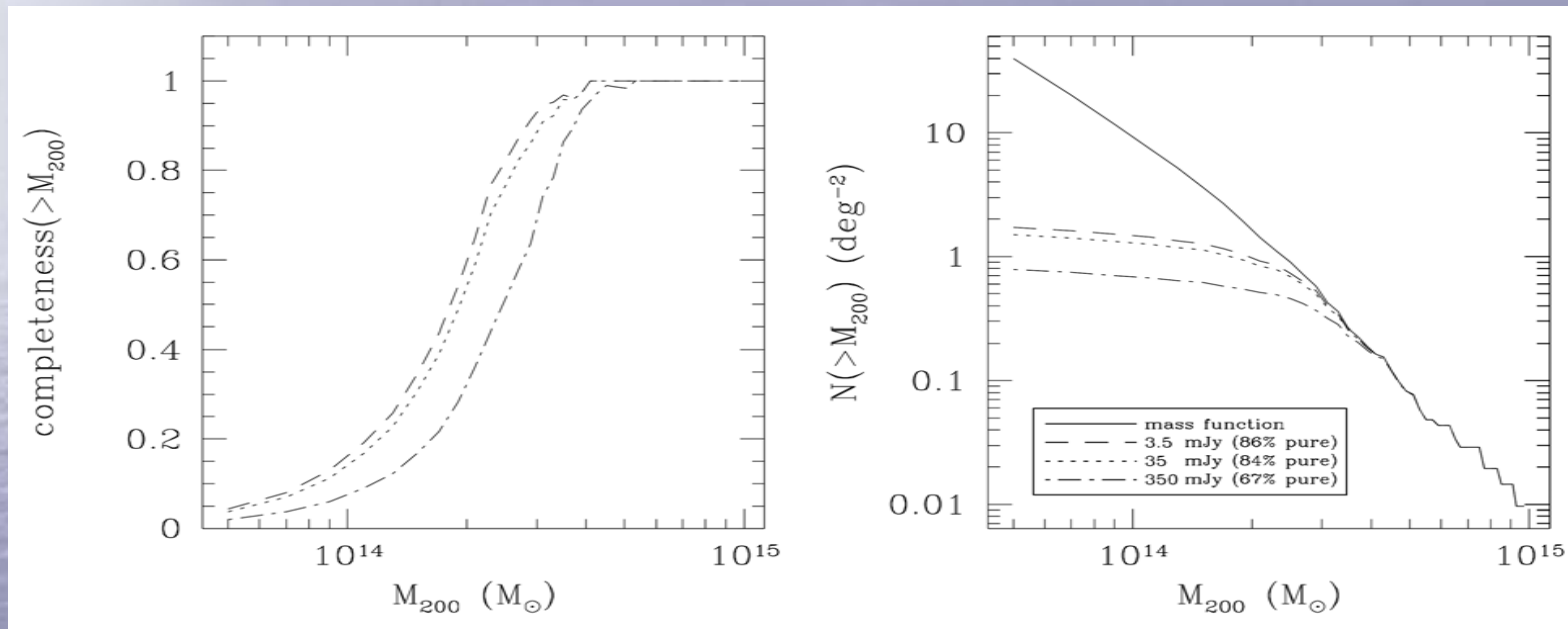


FIG. 9.— Completeness and purity when both infrared and radio sources are included. A $3\text{-}\sigma$ cut is used for all the curves. The different curves represent different flux cuts at 145 GHz for the radio sources. If all the radio sources above 3.5 mJy at 145 GHz are removed from the three-frequency ACT maps, then we recover the results with only infrared point sources included. Removing all sources above 35 mJy at 145 GHz gives results that are only slightly degraded compared to the former case.

3.5 mJy = 100 μ K / 35 mJy = 1000 μ K at 145 GHz in arcmin² beam

Sehgal et al. 2007, ApJ, 664

**ACT should find sample which is 90% complete above
3 x 10¹⁴ Msun and 85% pure, removing 1000 μ K sources.**

SZ Cluster Detection

Using thermal SZ power spectrum in filter different from that in simulation

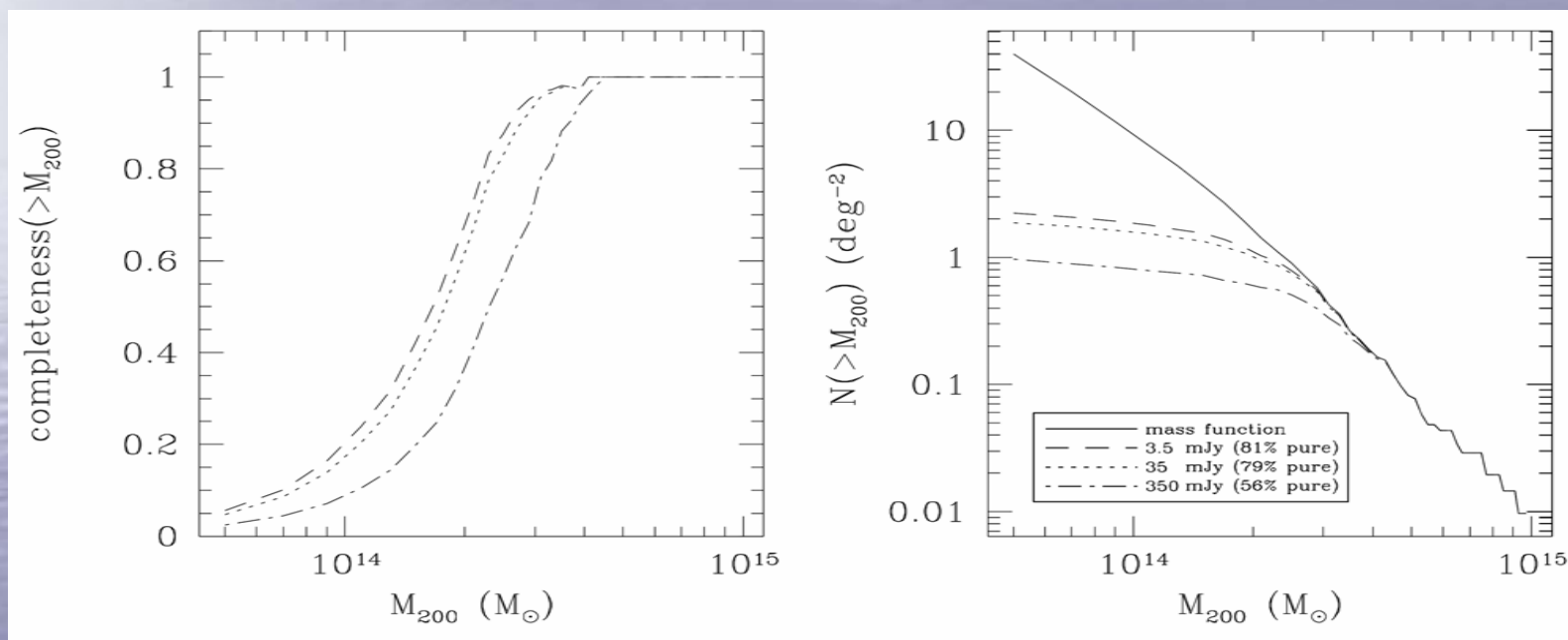


FIG. 10.— Completeness and purity of the detected cluster sample for the cases described in Figure 9, but this time using a filter constructed with a cluster Compton- y power spectrum derived analytically from Komatsu & Seljak (2002), instead of taken directly from the simulations. The completeness is slightly increased and the purity slightly decreased as compared to the previous Figure, but overall the difference is small.

Improvements to Simulations

New Simulations:

- 6 frequency bands/each strip 20 deg wide
- Thermal SZ/Kinetic SZ from full momentum and density field
- Lensed CMB
- IR/Radio Sources Correlated with Halos
- Catalogs of IR and Radio Sources
- Catalog of Halos and their Properties
- ICM SZ Signal has Relativistic Corrections
- Galactic Dust Emission

People involved: Hy Trac (CfA), Paul Bode (Princeton), Kevin Huffenberger (JPL/Caltech), Sudeep Das (Princeton), Carlos Hernandez-Monteagudo (Max-Planck, Garching), Yen-Ting Lin (Princeton/Catholica)

Improvements still to come:

- Refine point source prescriptions
- Add X-ray and optical maps

More Realistic SZ Cluster Detection with Simulations

- Run new simulations through ACT simulator
 - filter maps and detect clusters
- Characterize atmosphere detected by ACT and fold this into noise removal algorithm
- Investigate bias in the recovery of the integrated thermal SZ cluster signal

Conclusion

- Galaxy cluster surveys will provide a promising way to probe the nature of dark energy
- However, systematic uncertainties in cluster mass estimates and sample selection must be well understood
- Comparison of X-ray and weak-lensing cluster mass estimates from four DLS shear-selected clusters suggests agreement between mass estimates except if cluster is dynamically disrupted, in which case bias needs to be better understood
- Larger cluster samples in hand will shed more light on this
- Cluster selection study for ACT suggests ACT can find a cluster sample, via SZ effect, that is 90% complete above 3×10^{14} Msun and 85% pure
- Enhanced microwave simulations will probe this with greater accuracy and be made publicly available